

# The effect of nanostructural hierarchy on the mechanical properties of aluminium alloys during deformation processes

Li-Juan Hu · Shi-Jin Zhao

Received: 19 April 2012 / Accepted: 29 May 2012 / Published online: 12 June 2012  
© Springer Science+Business Media, LLC 2012

**Abstract** New generation of lightweight structures and technologies enables the development of materials to exhibit superior property combinations. In the present work, cellular automata is used to address the problem of dislocation behaviour and 4 factors: (i) a high density of dislocations, (ii) sub-nanometre intragranular solute clusters, (iii) 2 geometries of nanometre-scale intergranular solute structures and (iv) grain sizes tens of nanometres in diameter featuring in aluminium alloys containing a nanostructural hierarchy and exhibiting record strength with good ductility—an aerospace grade 7075 alloy exhibits a yield strength of 1 GPa and total elongation to failure of 9 %. We show that the clusters and geometries of nanometre-scale intergranular solute structures govern the strength of such material, resulting in their increasing elongation. Our results demonstrate that this simulation explains the phenomena of the super-strong materials of new generation with entirely new regimes of property-performance space.

## Introduction

Bulk nanostructured materials (NSM) processed by methods of severe plastic deformation (SPD) have attracted the growing interest of specialists in materials science [1–3]. There remains an unsatisfactory fit between theory-based structure and property in SPD metals. New experimentally derived insights into the nanostructure have

comprehensively described the structures (i.e. twins, grain boundaries with high angle misorientation) within these unusual materials and their influences on properties [1, 4–6]. In conventional metals, there is plenty of space for dislocations line defects the motion of which results in permanent material deformation to multiply so that the metal strengths are controlled by dislocation interactions with grain boundaries and other obstacles [7–9]. The unusual mechanical behaviour of nanocrystalline materials [10, 11], showing either greatly enhanced ductility [12–14] or dramatically increased strength, hardness and ductility at room temperature [15–18], is thought to arise from the intricate interplay between dislocation, grain-boundary processes and sub-nanometre structures. It is well known that heavy deformations, e.g. by SPD, can result in significant refinement of microstructure at low temperatures. Ultrafine-grained Al alloy with nanoscale solute structures embedded in individual grains and grain boundaries has recently been synthesized achieving a strength increase by a factor of 5–8 relative to conventional coarse-grained, as well as considerable ductility [6].

For nanocrystalline metals without nanoscale solute structures, molecular dynamics simulations [19, 20] have shown the mechanical behaviour as grain size is reduced to about 70 nm, which has been attributed to a transition from dislocation-mediated plastic deformation to grain boundary (GB)-associated mechanisms such as grain-boundary sliding, grain-boundary diffusion at different temperatures and grain rotation [19, 21–23]. Owing to the complexities of the nanostructures and deformation mechanisms, the dislocation behaviour has turned out to be very complex involving multiple mechanisms for the generation and annihilation of the defects in the nanostructural metals. Furthermore, collective phenomena may result from mutual interactions between dislocations and from interactions between

---

L.-J. Hu · S.-J. Zhao (✉)  
Key Laboratory of Microstructures, Institute of Materials  
Science, School of Materials Science and Engineering,  
Shanghai University, Shanghai 200072, China  
e-mail: shijin.zhao@shu.edu.cn

dislocations and other defects such as grain boundaries and intragranular solute clusters. The intricate interplay between dislocation and grain boundaries has a new twist for nanocrystalline materials, where the small grains put severe limitations on the dislocation behaviour [24–26].

### Simulation model

By means of a developed, massively cellular automata (CA) code for the simulation of polycrystal plasticity [27], here, we demonstrate for the case of nanocrystalline Al alloy the complex interplay of various dislocation, grain-boundary and nanoscale solute structures responsible for the room-temperature deformation behaviour of materials with nanometre grain size. A unique aspect of our work, arising from our ability to deform to rather large plastic strains and to consider a relatively large amount grains, is the observation of deformation under very high dislocation densities and nanoscale solute structures. We are thus able to identify the intra- and inter-granular dislocation and sub-nanometre intragranular solute clusters and 2 geometries of nanometre-scale intergranular solute structures in a deformation regime where they compete on an equal footing and to gain nano-level insights into the underlying mechanisms not currently possible experimentally. These insights include the observation of mechanical enhancing about solute clusters, structures and the effect of volume fraction in which contains the sub-nanometre intragranular solute clusters and 2 geometries of nanometre-scale intergranular solute structures during the deformation. Our simulations thus illustrate the manner in which dislocation-based deformation of nanocrystalline materials differs qualitatively from the well-studied behaviour of coarse-grained materials.

We assume that a NC material with a grain size of  $d$  consists of a mixture of a crystalline-grain interior, which has high density of dislocations and a grain-boundary layer having a width of  $w$ . The grain-boundary width is approximately 3 times the Burgers vector ( $b$ ), i.e.  $w \approx 3b$ . The volume fraction of the grain-boundary layer ( $f$ ) can be expressed by [28]

$$f = \frac{g_1(d/2)^3 - g_1(d/2 - w/2)^3}{g_1(d/2)^3} = 1 - \left(1 - \frac{w}{d}\right)^3 \quad (1)$$

where  $g_1$  is defined as a constant the value of which depends on the grain morphology. For a spherical grain,  $g_1$  is  $4\pi/3$ , and for a circle grain,  $g_1$  is  $\pi$ . The volume fraction of the grain-boundary layer increases very rapidly by decreasing the grain size when the grain size is less than 40 nm.

It is assumed that the flow equations of a NC material consisting of a crystalline-grain interior including sub-nanometre intragranular solute clusters (denoted by  $l$ ) and a grain-boundary layer (denoted by  $b$ ), in which the grain-boundary layer includes the general layer and nanometre-scale intergranular solute structures, follow a simple rule of mixtures, i.e.

$$\sigma = (1 - f)\sigma_l + f\sigma_b \quad (2)$$

$$\varepsilon = (1 - f)\varepsilon_l + f\varepsilon_b \quad (3)$$

where  $\sigma$ ,  $\sigma_l$  and  $\sigma_b$  (or  $\varepsilon$ ,  $\varepsilon_l$  and  $\varepsilon_b$ ) are the stresses (or strains) of a nc material, crystalline-grain interior and grain-boundary layer, respectively. When  $\sigma = \sigma_l = \sigma_b$ , the above equations reduce to the equal stress condition of the composite materials, while these two equations reduce to the equal strain condition if  $\varepsilon = \varepsilon_l = \varepsilon_b$ . The derivatives of Eqs. 2 and 3 with respect to time,  $t$ , lead to the stress rate,  $\dot{\sigma}$  and strain rate,  $\dot{\varepsilon}$ , of the NC material expressed by the respective components to the grain interior and GB, i.e.

$$\dot{\sigma} = (1 - f)\dot{\sigma}_l + f\dot{\sigma}_b \quad (4)$$

$$\dot{\varepsilon} = (1 - f)\dot{\varepsilon}_l + f\dot{\varepsilon}_b \quad (5)$$

A topic of active investigations remains in the structure of grain boundaries in NC materials. The structural information of grain boundaries in NC materials has been obtained by both high resolution TEM and computer simulations. The structure of NC materials is still under active debate, whereas this issue has been clarified by tremendous efforts. One of the theories regarding the structure of grain boundaries is that the GB is composed of a layer of amorphous phase with disordered atomic arrangements. It was concluded that grain boundaries in NC Pd and Si with high energy bicrystalline grain boundaries consist of a glassy, glue-like intergranular phase by molecular dynamic simulation [29–31]. The existence of an amorphous state in pure metals has been confirmed both experimentally and theoretically [32–36] except for amorphous alloys in the binary systems being reported [37–40]. In the current model, the grain-boundary layer of the NC materials is assumed to be a glassy structure. Owing to a low glass-transition temperature (close to or even lower than room temperature), the plastic deformation of amorphous metals and alloys with a simple chemistry may show a viscoelastic flow at room temperature. Van Swygenhoven and Caro [41] have assumed a nonlinear viscoplastic deformation at the GB for the NC materials. Here, it was assumed that a viscoelastic deformation is responsible for the plastic deformation in the amorphous grain-boundary layer. The plastic deformation of viscoelastic solid is described by a differential constitutive equation based on a Maxwell model [42], which has been proven to be very useful when rationalizing the stress

relaxation of a viscoelastic solid with a single characteristic relaxation time [43, 44], i.e.

$$\dot{\sigma}_b = E_b \dot{\varepsilon}_b - \frac{\sigma_b}{t_b} \quad (6)$$

where  $\dot{\sigma}_b$ ,  $E_b$ ,  $\dot{\varepsilon}_b$  and  $t_b$  are the stress rate, Young's modulus, strain rate and relaxation time of grain-boundary layer, respectively.

In the following text, some assumptions were made to solve Eq. 6. It is assumed that an elastic deformation for the grain interior during plastic deformation since the crystalline-grain interior including solute cluster is free from dislocations. In order to avoid the debonding of the interfaces, a shear stress ( $\tau_b$ ) must be developed between the interfaces of the grain interior and the grain-boundary layer when a NC material is strained. Therefore, a normal stress in the grain interior ( $\sigma_l$ ) is built up, which is transmitted from the GB to the grain interior by means of the shear stress ( $\tau_b$ ). The relationship between  $\sigma_l$  and  $\tau_b$  can be expressed by [45]

$$\sigma_l = g_2 \tau_b \quad (7)$$

with  $g_2$  is the geometric factor depending on the shape of the grain. The Newtonian viscosity of the grain-boundary layer, i.e.  $\eta_b$  is determined by the normal stress ( $\sigma_b$ ) and the strain rate ( $\dot{\varepsilon}_b$ ):

$$\eta_b = \frac{\sigma_b}{\dot{\varepsilon}_b} \quad (8)$$

The shear stress depends not only on the normal stress, but also on its direction. The maximum shear stress is  $\tau_b = \sigma_b/2$  for homogenous solids. For simplicity, it is assumed that the shear stress is the same at all directions [45] and is described by

$$\tau_b = g_3 \sigma_b \quad (9)$$

where  $g_3$  being another geometric factor. For a viscoelastic solid, the relaxation time ( $t_b$ ) in Eq. 6 is related to the Newtonian viscosity as expressed by

$$t_b = \frac{\eta_b}{E_b} \quad (10)$$

A combination of Eqs. 7 through 10 yields

$$\sigma_l = g_2 g_3 E_b t_b \dot{\varepsilon}_b \quad (11)$$

According to Hooke's law for the elastic solid of the grain interior, the strain of the grain interior ( $\varepsilon_l$ ) is given by  $\varepsilon_l = \sigma_l/E_l$ . Therefore,

$$\varepsilon_l = \frac{g_2 g_3 E_b t_b \dot{\varepsilon}_b}{E_l} \quad (12)$$

Differentiation of Eq. 12 with respect to the time ( $t$ ) leads to

$$\dot{\varepsilon}_l = \frac{g_2 g_3 E_b t_b}{E_l} \ddot{\varepsilon}_b \quad (13)$$

Following Eq. 5, the strain rate of the grain-boundary layer is given by

$$\dot{\varepsilon}_b = \frac{\dot{\varepsilon}}{f} (1 - e^{\frac{f}{c(\dot{\varepsilon}-1)}}) \quad (14)$$

where  $c = (g_2 g_3 E_b t_b)/E_l$ . Substituting Eq. 11 into 2 arrives at an expression for the normal stress of the GB by

$$\begin{aligned} \sigma_b &= \frac{\sigma - (1-f)g_2 g_3 E_b t_b \dot{\varepsilon}_b}{f} \\ &= \frac{\sigma - (\frac{1}{f} - 1)(1 - e^{\frac{f}{c(\dot{\varepsilon}-1)}})g_2 g_3 E_b t_b \dot{\varepsilon}}{f} \end{aligned} \quad (15)$$

A derivative of  $\sigma_b$  in Eq. 15 with respect to  $t$ , assuming a constant strain rate, leads to

$$\dot{\sigma}_b = \frac{\dot{\sigma}}{f} - \frac{g_2 g_3 E_b t_b \dot{\varepsilon}}{f c} e^{\frac{f}{c(\dot{\varepsilon}-1)}} \quad (16)$$

Equations 15 and 16 imply that the stress rate of the crystalline-grain interior is not 0. The previous results indicate that the elastic-grain interior has contributions to the overall strain rate and stress rate. Therefore, the strain rate and stress rate of the grain-boundary layer are not equal to those of the NC material divided by the volume fraction of the grain-boundary layer.

Substituting Eqs. 14–16 into Eq. 6 leads to the flow equation of a NC material given as

$$\begin{aligned} \dot{\sigma} &= \frac{g_2 g_3 E_b t_b \dot{\varepsilon}}{c} e^{\frac{f}{c(\dot{\varepsilon}-1)}} - \frac{\sigma}{t_b} + E_b \dot{\varepsilon} \\ &\quad \times (1 - e^{\frac{f}{c(\dot{\varepsilon}-1)}}) \left( 1 + \left( \frac{1}{f} - 1 \right) g_2 g_3 \right) \end{aligned} \quad (17)$$

The solution of Eq. 17 is given as

$$\sigma = e^{\frac{-t}{t_b}} \left( \frac{GGG - E_b \dot{\varepsilon}^2 GG}{1 + G t_b} t_b (e^{\frac{1+G t_b t}{t_b}} - 1) + E_b \dot{\varepsilon} G G t_b (e^{\frac{t}{t_b}} - 1) \right) \quad (18)$$

where  $G = \frac{f}{c(\dot{\varepsilon}-1)}$ ,  $GG = \left( 1 + \left( \frac{1}{f} - 1 \right) g_2 g_3 \right)$ ,  $GGG = E_l \dot{\varepsilon}$ .

Equation 18 indicates that the stress relaxation of a NC material is related to the viscosity of the GB, the strain rate, the shape of the grain, the time, the grain interior modulus as well as the volume fraction of the grain-boundary layer.

Deformation of nanocrystals has previously been investigated by means of molecular dynamics simulations [46, 47]. To represent real material structures seen in experiments as closely as possible [6], we have performed simulations on fully two-dimensional polycrystals with subnanometre intragranular solute clusters and two geometries of nanometre-scale intergranular solute structures.

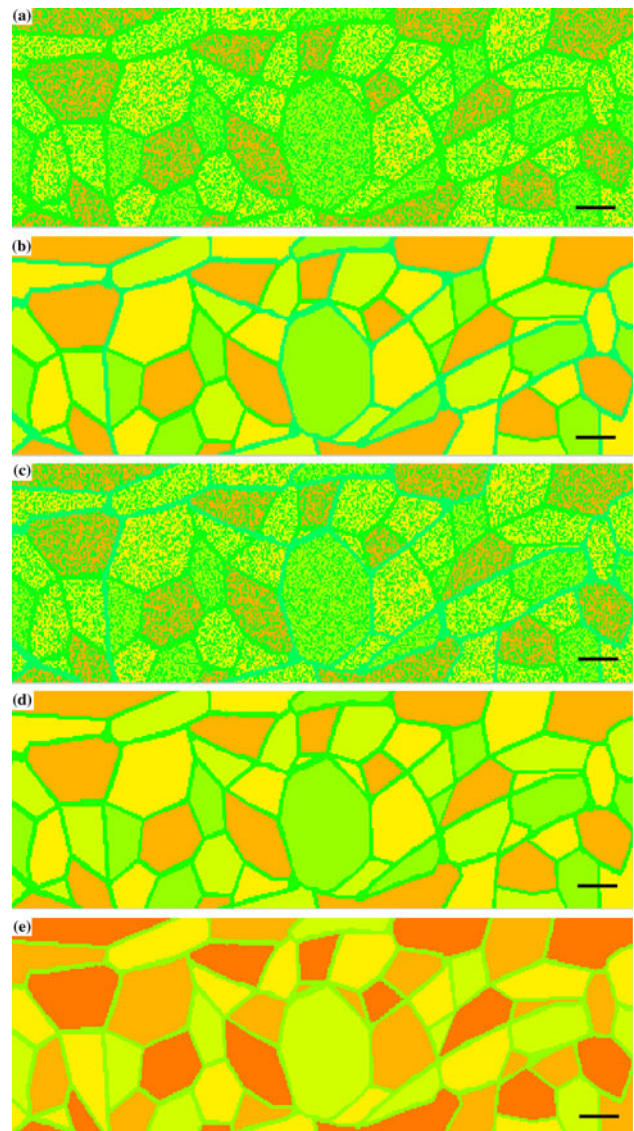
The simulations are performed on two-dimensional polycrystal samples containing 18 randomly orientated

Voronoi grains. In each grain, sub-nanometre intragranular solute clusters are inserted by nucleating and growing randomly in the matrix according to CA. Moreover, the volume fraction of solute cluster in grain, lineal solute and nodal solute are 38.49, 8.33 and 1.87 %, respectively. The typical shapes of the nanoscale solute inclusion, i.e. solute cluster, lineal solute and nodal solute are circular, linear and approximately triangular, respectively. The samples with  $d = 25$  nm have dimensions of  $360 \times 125$  nm<sup>2</sup> containing about 35 grains. Four samples with initial uniform structure of two geometries of nanometre-scale intergranular solute and sub-nanometre intragranular solute clusters are simulated. The local dislocation density is used to identify different grains during deformation in which the typical range of dislocation density is  $6.9 \times 10^{15}$ – $3.7 \times 10^{16}$  m<sup>-2</sup>. In order to compare with the macro-properties, the dislocation is converted to flow stress displaying in the figures. Furthermore, the nodal and lineal solute structures are inserted by nucleating and growing in the grain boundaries, which are similar to the experimental result [6]. Young's modules of matrix and solute clusters are 71.9 and 77.3 GPa [35], respectively. Ten types of contour bars are painted in colour to distinguish the stress. Deformation patterns of four samples with different grain-boundary layer and cluster in grain interior and GB, but the same grain size  $d = 25$  nm and the contrast to another sample with large grain size treated by T6 are shown in Fig. 1.

## Results and discussion

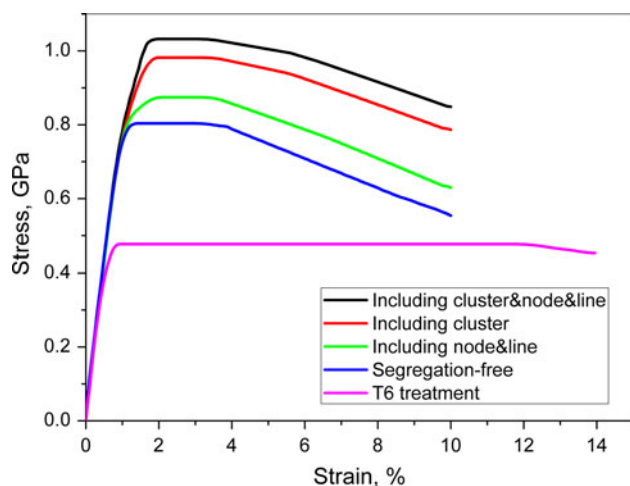
The observation of nanoscale solute cluster and nodal and lineal structures in a nanocrystalline material is very surprising [6] not only because of the very small grain size but also because Al alloy has a high strength and preferable elongation. Our simulations reveal entirely different mechanism for deformation of Al alloy by high pressure torsion (HPT). This mechanism involves the dislocation density increasing in a grain-boundary segment and motion-impeding effect of solute clusters to dislocation. In addition, Fig. 1a and c reveals the mechanism observed earlier [48] for the strength distributions associated with obstacle in the materials. In contrast with the mesostructure of obstacle, it is known that dislocation circling nanoscale solute clusters require extremely large local stresses.

Existence of different upper yield point and steady stage occurs in the stress–strain curves from CA simulations. Figure 2 displays the deformation curves for different microstructures at an applied uniaxial tension. The different upper yield point in the stress–strain curves from CA simulations is associated with the dislocation obstacle of different precipitates in the initially dislocation-unfree



**Fig. 1** Initial model of cellular automata showing the aluminium alloy. Four structures of aluminium alloy exhibiting record properties and solute nanostructure hierarchies (NH-7075). **a** A model of the nanostructure including nanoscale solute clusters. **b** Nanostructure including nodal and lineal solute structures. **c** Nanostructure including clusters, nodal and lineal structures. **d** Nanostructure without clusters and nodal and lineal solute structures. **e** T6-7075 aluminium. Scale bar in **a–d** 25 nm, in **e** 3  $\mu$ m

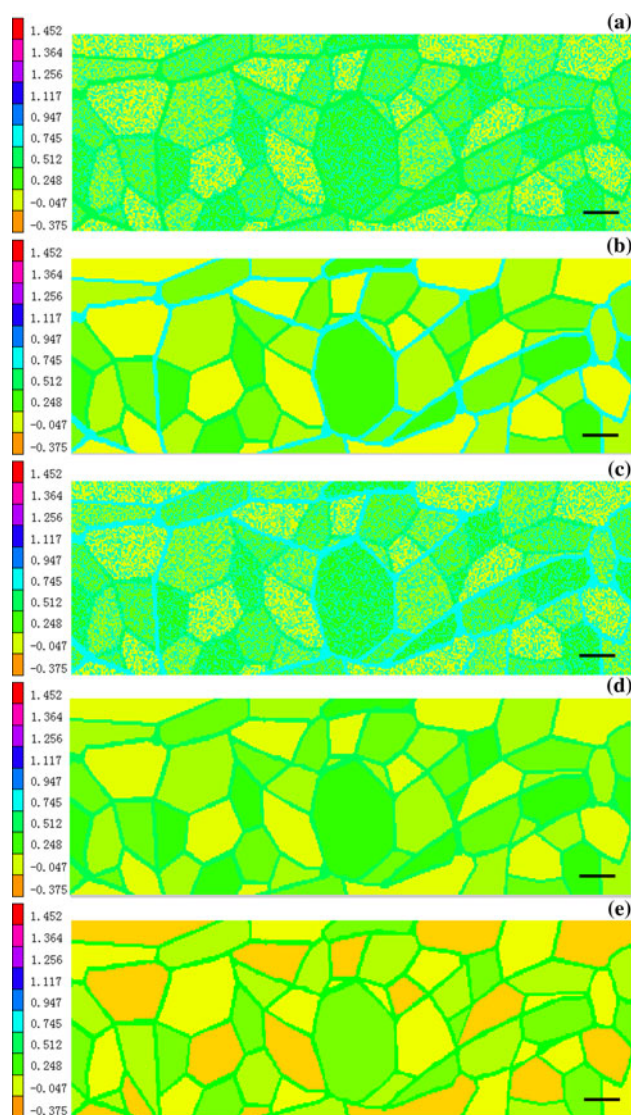
samples. At this point, the macroscopic stress reaches a critical value to activate a large number of dislocations for plastic deformation. The subsequent stresses keep steady due to the obstacle of clusters. As the plastic strain increases, the dislocation concentration in the grain interiors continues to increase. Therefore, the stress elevates with the dislocation increasing in Figs. 3, 4, and 5 in which grains are differently coloured representing stress distribution with the remaining figures displaying the grains according to their local stress. From Fig. 4, it can be seen that the colour



**Fig. 2** Stress-strain curves from Cellular Automata simulations of nanostructural hierarchies aluminium alloy. Simulated stress–strain curves for nanostructure hierarchies aluminium alloy with nanoscale solute clusters, nano-nodal and lineal structures, nanoscale clusters and nodal and lineal structures, no precipitates in the structures and T6-7075 aluminium alloys, respectively

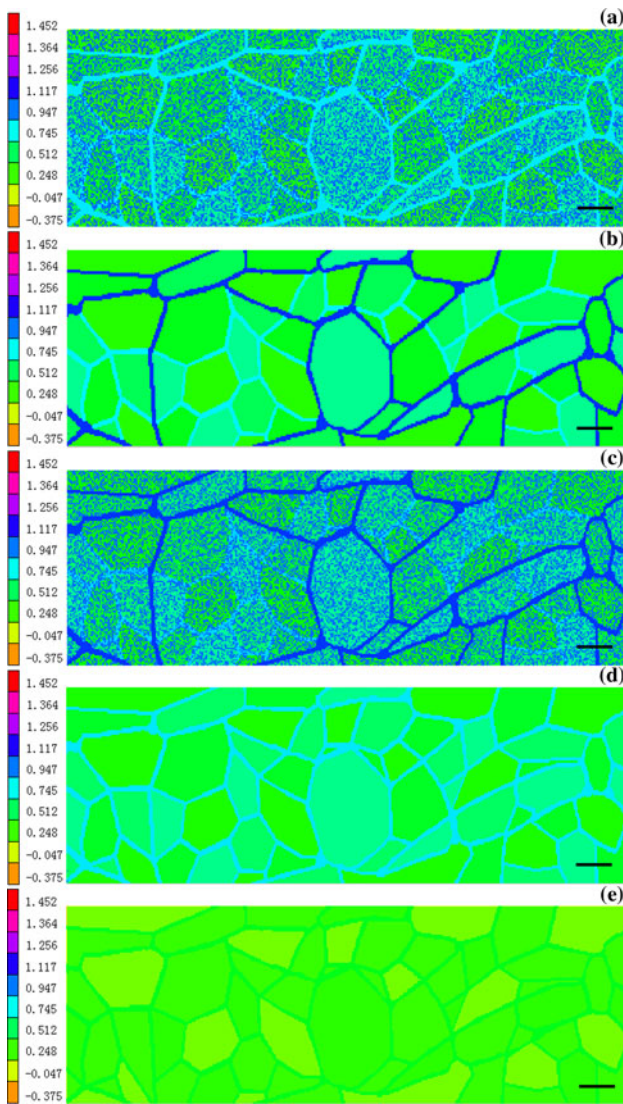
bar indicates that the stress of sub-nanometre solute structures and nanoscale nodal and lineal structures increase rapidly. It can be confirmed that pile-up of dislocation along nodal and lineal nanostructures, while dislocations intersect with solute clusters for small solute atoms from Fig. 3, 4, and 5. Such dislocation mechanism transition results in the increase of yield strength in nanostructural Al. It has been shown in the literature that the strain-compensated clusters can make elastic stresses prevent phase separation [49], which is negligible compared to the magnitude of stress shown in Fig. 2. Therefore, once the solute clusters are nucleated, they could prevent dislocation gliding along intracrystalline. If the critical stress to drive parallel dislocation motion is so large, the solute cluster will prevent this mechanism from domination deformation at all intracrystalline. Our simulations show that yield stress is mainly controlled by the sub-nanometre intragranular solute clusters, while at higher grain-boundary curvature and grain-boundary junction points nanometre-scale intergranular nanostructures, there are more insufficient operative increase for yield stress than the sub-nanometre intragranular solute clusters even if their scale is large.

Table 1 provides a summary of the mechanical properties across the hierarchy of nanostructures in this study and experiment [6]. It can be also confirmed that cluster is the most important factor to improve the strength of aluminium alloy processed by HPT. In addition, lineal and nodal structure is lesser to elevate the strength of alloy. In addition, it can be seen that the simulation result including cluster, lineal and nodal structures is in good agreement with the experimental result of nanostructures.



**Fig. 3** Early stages of the deformation of the leading partial stress at strain = 0.25 %: **a** nanostructure including nanoscale solute clusters, **b** nanostructure including nodal and lineal solute structures, **c** nanostructure including clusters, nodal and lineal structures, **d** nanostructure without clusters and nodal and lineal solute structures, **e** T6-7075 aluminium. Scale bar in **a–d** 25 nm, in **e** 3  $\mu\text{m}$

The simulation allows further investigation of details of the strengthening process about different nanostructural details. Strain in local grain and GB versus stress is plotted in Fig. 6. Figure 6a shows the stress–strain curves of one grain excluding the effect of GB. It can be seen that the stress of one grain including cluster is higher than other structures' stress. According to the simulation model, the volume fraction of cluster is more than that of lineal and nodal structures. Therefore, the effect of strength from cluster is more apparent than that of lineal and nodal structures. Figure 6b shows the computational stress–strain curves including the effect of nanocrystalline-GB.



**Fig. 4** Elastic stages of deformation at strain = 0.75 %: **a** nanostructure including nanoscale solute clusters, **b** nanostructure including nodal and lineal solute structures, **c** nanostructure including clusters, nodal and lineal structures. **d** Nanostructure without clusters and nodal and lineal solute structures, **e** T6-7075 aluminium. Scale bar in **a–d** 25 nm, in **e** is 3 μm

Including the effect of GB, it shows beneficial effects in terms of enhancing flow strength of lineal and nodal structures, while the flow strength of cluster decreasing. The strength of lineal and nodal structures may benefit from increasing the GB. However, it results in decreasing in strength of cluster with increasing the GB. Therefore, the optimization strategy is straightforward in terms of balance between reducing and increasing GB.

The significant body of nanostructural Al in simulations described above suggests important similarities and some differences between the GBs of local grain including and excluding in nanocrystalline microstructures. However, more different effects of GBs are shown in local grain and

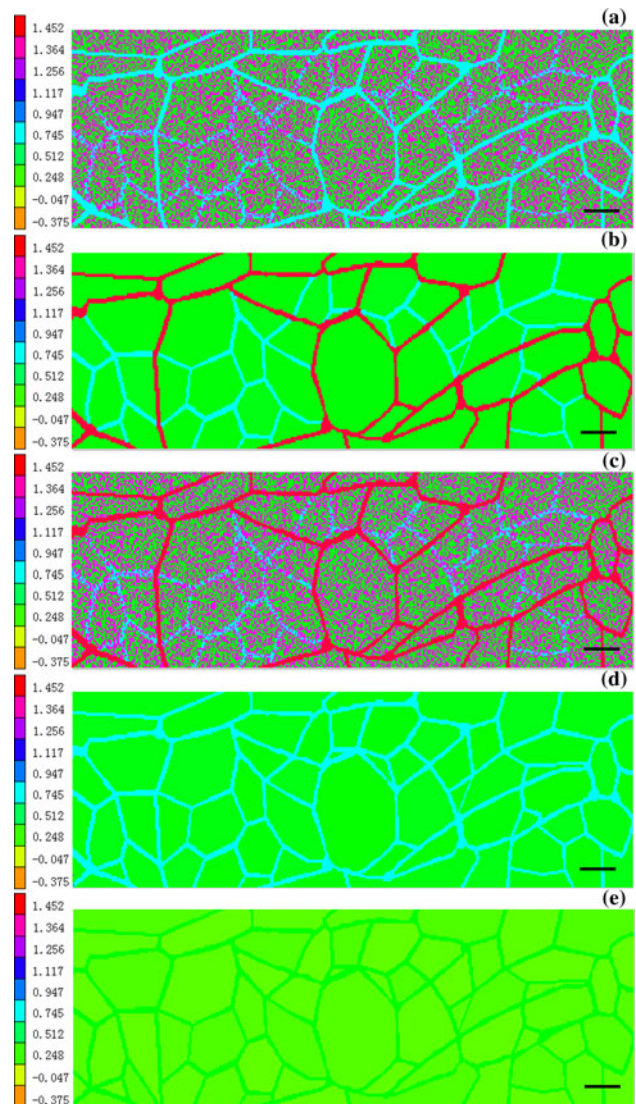


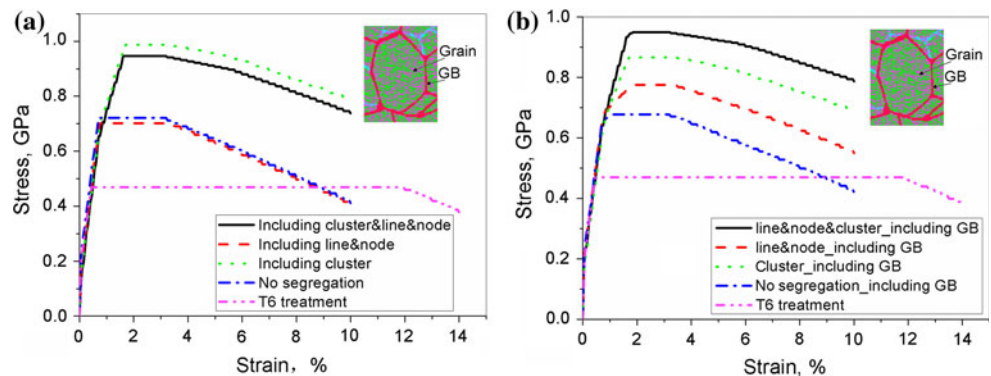
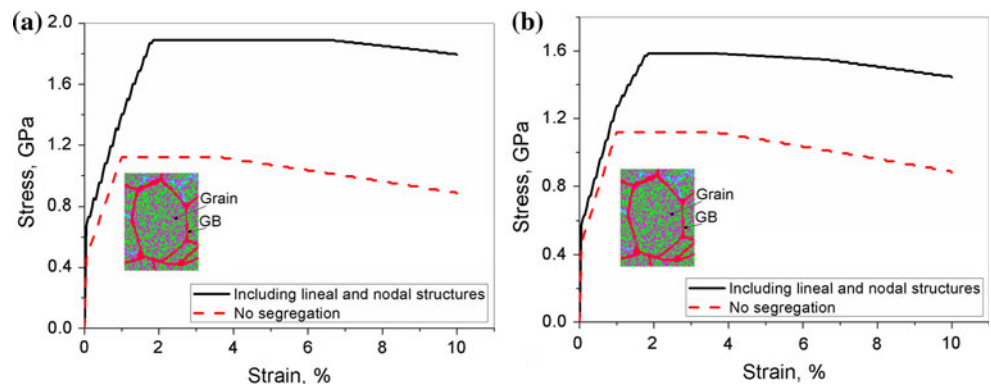
**Fig. 5** Snapshot of deformation stage of strain = 9.5 % of **(a–d)** and the strain = 13.45 % of **(e)** from the simulation: **a** nanostructure including nanoscale solute clusters, **b** nanostructure including nodal and lineal solute structures, **c** nanostructure including clusters, nodal and lineal structures. **d** Nanostructure without clusters and nodal and lineal solute structures, **e** T6-7075 aluminium. Scale bar in **a–d** 25 nm, in **e** 3 μm

total grains. Figure 7 shows the stress–strain curves of GB according to one grain and whole simulation model. As evidenced by the observation in Fig. 7, the structures of GB in nanocrystalline microstructure are important to strengthen nanostructural Al. The strength of GB in one grain is extremely higher than that of whole simulation model. Therefore, it can be seen that the statistic stress of GB in grains in simulation model is lower than that of one grain GB.

In order to gain an understanding of the nanostructure of this difference, it is needed to look in more details into the nature of the model material and how this is reflected in the

**Table 1** Comparison of stress between different structures in this study and test results

	0.2 %YS (GPa)	UTS (GPa)	UE (%)
Line and node and cluster	1.02805	1.03224	6
Line and node	0.83408	0.8744	4
Cluster	0.88247	0.98179	4.5
No segregation	0.79585	0.80374	3.6
T6 treatment	0.58757	0.58757	11.95
test result of nanostructures	1.022	1.05	5
Test result of T6 treatment	0.485	0.520	12

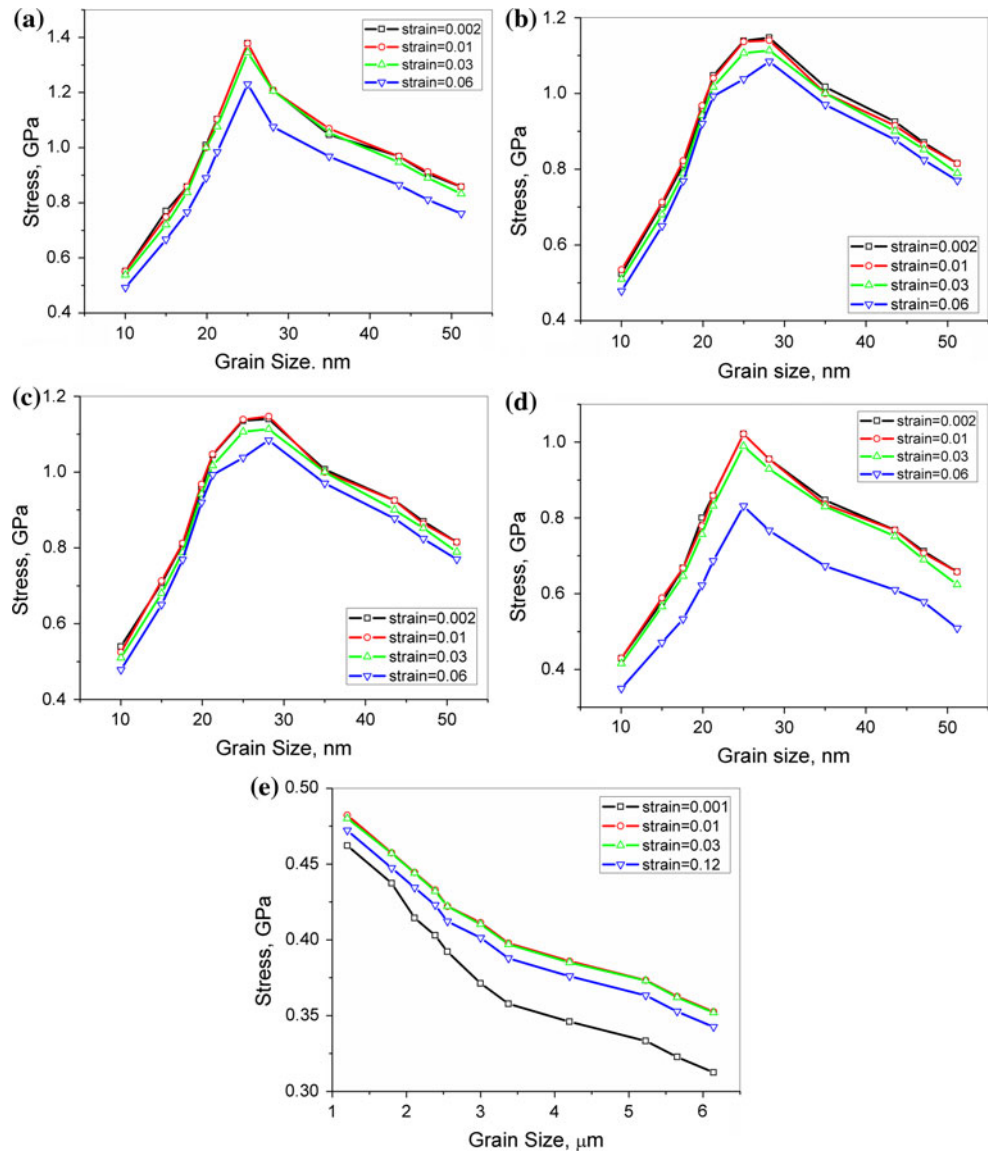
**Fig. 6** Comparison of stress–strain in local one grain: **a** intracrystalline, **b** including intracrystalline and grain boundary (GB)**Fig. 7** Comparison of the enhancement of one grain boundary and all grain boundaries: **a** including one grain boundary corresponding to the grain and grain boundary, **b** including all grain boundaries in simulation model

stress by investigating the grain size versus stress at different deformation stage. Figure 8 shows the local stresses as a function of grain size at four different stages of deformation corresponding to macro strain of 0.001, 0.01, 0.03 and 0.06 with nanoscale grain size, and 0.12 with micrometre grain size. This represents the stress gained as a function of grain size. Stress varies during the tensile process and shows similar tendency besides value at variant strains. It can be seen that the change tendency of the stress is more identical besides the values in Fig. 8a and d. Therefore, the curves in Fig. 8a and d exist a same critical grain size, which is about 25 nm and it is different with other researches [50–52] in which the yield stress peaks in many cases at an average grain size value on the order of 10 nm or so. From this result, it can be inferred that this discrepancy is induced by the solute cluster and linear and

nodal solute existing in the material. In contrast, little difference of change tendency exists in the curves between Fig. 8b and c. That is, the effect of cluster on the strength of nanostructural Al is same to the lineal and nodal structure. Compared with the curves in Fig. 8e, it can be confirmed that stresses of all nanostructures follow inverse Hall–Petch relation, while stresses of structure of micrometre follows Hall–Petch relation.

Our simulations mostly cover new ground, as yet experimentally unexplored, not only as far as the small grain size is concerned but also in other important aspects, such as solute clusters and nodal and lineal structures. In simulations on samples with different structures, a lot of dislocations interact with each other at the nanoscale solute cluster and nodal and lineal structures leading to the formation of dislocation junctions, which play an essential

**Fig. 8** Predicted local stresses as a function of grain size at four different stages of deformation corresponding to macro strain of 0.001, 0.01, 0.03 and 0.06 with nanoscale grain size, and 0.12 with micrometer grain size. Microstructure: **a** including cluster, lineal and nodal structures, **b** including cluster, **c** including lineal and nodal structure, **d** no segregation, **e** T6 treatment



role in the strain hardening of deforming grains [53]. In contrast with high resolution transmission electron microscopy (HRTEM) and three dimensional atom probe tomography (3DAPT) experiments, the insights gained from Figs. 3, 4, and 5 inherently capture bulk deformation behaviour. Also, even for coarse-grained materials, it would be extremely difficult to extract the underlying deformation mechanisms from experiments in the type of dynamical detail available from Figs. 3, 4, and 5. Figure 9 shows direct evidence that the cluster number density and percentage are distributed in the sample. The occurrence of randomly occurring solute clusters was assessed by statistical estimation. A high concentration of clusters sized 5–13 solute atoms are observed to occur preferentially in Fig. 9a. The experimentally observed frequency of solute clusters had the expected random occurrences subtracted [6]. In Fig. 9b, it can be seen that the tendency of

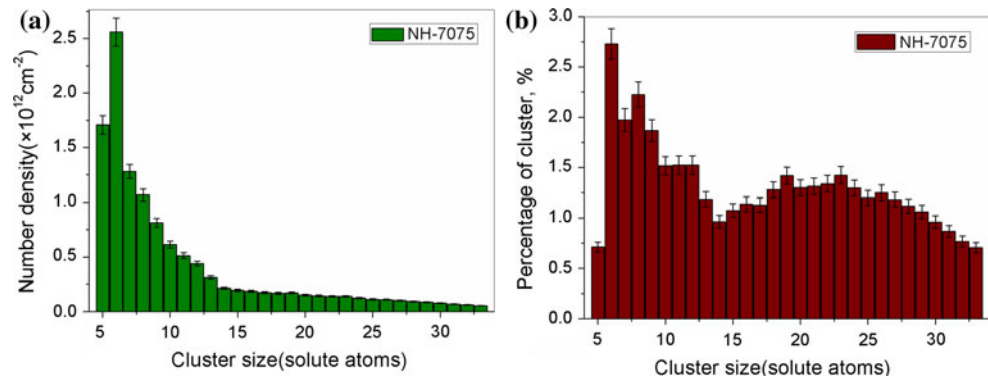
percentage of intra-granular solute clusters, in which exist two high concentrations of clusters sized 6–13 and 18–27 solute atoms observed to occur preferentially, is different with the cluster size. Although the tendency is different, the results also reflect that the 5–13 solute atoms are the main concentration in the NH-7075 alloy, while the percentage of 18–27 solute atoms is obvious due to their larger size in Fig. 9b. This analysis reveals that clusters in the model are similar with the experimental results [6].

### Conclusions

The above simulations of well-characterized, although highly idealized, model systems illustrate the opportunities offered by CA simulations towards unravelling the complex interplay between dislocation and nanoscale solute



**Fig. 9** Number density and percentage of intra-granular solute clusters in the NH-7075 alloy: **a** number density versus cluster sizes, **b** percentage of intra-granular solute clusters versus cluster sizes



clusters and structures in nanocrystalline materials. For fundamental studies, the topic of current interest is investigations focusing on the effect of nanoscale cluster and geometries of nanometre-scale intergranular solute structures in aerospace grade 7075 alloy with hierarchy of nanostructures. This simulation yield stress is mainly controlled by the sub-nanometre intragranular solute clusters, while at higher grain-boundary curvature and grain-boundary junction points which are nanometre-scale intergranular nanostructures, there are more insufficient operative increase for yield stress than the sub-nanometer intragranular solute clusters even if their scale is large. Investigation of the occurrence of stresses in local grain including and excluding GB should provide guiding information on the role of GB during plastic deformation. The optimization strategy of nanostructure of 7075 Al alloy is straightforward in terms of balance between reducing and increasing GB. According to the stresses versus grain size curves, stresses of all nanostructures follow inverse Hall–Petch relation, while stresses of structure of micrometre follows Hall–Petch relation. In this study, a good agreement between experiment and simulation has been obtained for the effect of hierarchy of nanostructures.

**Acknowledgement** The supports of the Key Project of Natural Science Foundation of China Grant No. 50931003, the Shanghai Committee of Science and Technology Grants No. 09520500100 and 10PJ1403900, the Key Project of Innovation Program of Shanghai Municipal Education Commission Grant No. 10ZZ62, and Shu Guang Project Grant No. 09SG36 are gratefully acknowledged.

## References

- Valiev RZ, Islamgaliev RK, Alexandrov IV (2000) *Prog Mater Sci* 45:103
- Valiev RZ (2007) *J Mater Sci* 42:1483. doi:10.1007/s10853-006-1281-3
- Liu M, Roven HJ, Liu X, Murashkin M, Valiev RZ, Ungár T, Balogh L (2010) *J Mater Sci* 45:4659. doi:10.1007/s10853-010-4604-3
- Hassani FZ, Ketabchi M, Hassani MT (2011) *J Mater Sci* 46:7689. doi:10.1007/s10853-011-5748-5
- Murashkin M, Kil'mametov AR, Valiev RZ (2008) *Phys Metal Metal* 106:90
- Liddicoat PV, Liao XZ, Zhao YH, Zhu YT, Murashkin MY, Lavernia EJ, Valiev RZ, Ringer SP (2010) *Nature Commun* 1:1
- Hall EO (1951) *Proc Phys Soc Lond B* 64:747
- Friedel J (1967) *Dislocation*. Pergamon, Oxford
- Hirth J, Lothe J (1992) *Theory of dislocations*. Krieger, Malabar
- Tjong SC, Chen H (2004) *Mater Sci Eng R* 45:1
- Meyers MA, Mishra A, Benson DJ (2006) *Prog Mater Sci* 51:427
- Karch J, Birringer R, Gleiter H (1987) *Nature* 330:556
- McFadden SX, Mishra RS, Valiev RZ, Zhilyaev AP, Mukherjee AK (1999) *Nature* 398:684
- Kim BN, Hiraga K, Morita K, Sakka Y (2001) *Nature* 413:288
- Siegel RW (1997) *Mater Sci Forum* 235–238:851
- Morris DG, Morris MA (1997) *Mater Sci Forum* 235–238:861
- Nesladek P, Veprek S (2000) *Phys Status Solidi A* 177:53
- Valiev RZ, Murashkin MY, Kilmametov A, Straumal B, Chinh NQ, Langdon TG (2010) *J Mater Sci* 45:4718. doi:10.1007/s10853-010-4588-z
- Yamakov V, Wolf D, Phillpot SR, Mukherjee AK, Gleiter H (2002) *Nature Mater* 1:45
- Gerlich AP, Yue L, Mendez PF, Zhang H (2010) *Acta Mater* 58:2176
- Shan Z, Stach EA, Wiezorek JMK, Knapp JA, Follstaedt DM, Mao SX (2004) *Science* 30:654
- Kumar KS, Suresh S, Chisholm MF, Horton JA, Wang P (2003) *Acta Mater* 51:387
- Zhang H, Srolovitz DJ, Douglas JF, Warren JA (2009) *PNAS* 106:7735
- Van Swygenhoven H, Derlet PM, Frøseth AG (2006) *Acta Mater* 54:1975
- Bobylev SV, Mukherjee AK, Ovid'ko IA (2009) *Scripta Mater* 60:36
- Ni S, Wang YB, Liao XZ, Alhajeri SN, Li HQ, Zhao YH, Lavernia EJ, Ringer SP, Langdon TG, Zhu YT (2011) *Scripta Mater* 64:327
- Nabarro FRN (2006) *Acta Mater* 54:263
- Fan GJ, Choo H, Liawa PK, Lavernia EJ (2005) *Mater Sci Eng A* 409:243
- Kebllinski P, Phillpot SR, Wolf D, Gleiter H (1997) *Acta Mater* 45:987
- Kebllinski P, Wolf D, Phillpot SR, Gleiter H (1999) *Scripta Mater* 41:631
- Nagamanasa KH, Gokhale S, Ganapathy R, Sood AK (2011) *Proc Natl Acad Sci USA* 108:11323
- Cheng JB, Liang XB, Xu BS, Wu YX (2009) *J Non-Cryst Solids* 355:1673
- Zhang JZ, Zhao YS (2004) *Nature* 430:332
- Furuichi H, Ito E, Kanno Y, Watanabe S, Katsura T, Fujii N (2001) *J Non-Cryst Solids* 279:215

35. Soler JM, Beltrán MR, Michaelian K, Garzón IL, Ordejón P, Sánchez-Portal D, Artacho E (2000) *Phys Rev B* 61:5771
36. de la Fuente OR, Soler JM (1998) *Phys Rev Lett* 81:3159
37. Ophus C, Lubber EJ, Edelen M, Lee Z, Fischer LM, Evoy S, Lewis D, Dahmen U, Radmilovic V, Mitlin D (2009) *Acta Mater* 57:4296
38. Trelewicz JR, Schuh CA (2007) *Acta Mater* 55:5948
39. Schuh CA, Nieh TG, Iwasaki H (2003) *Acta Mater* 51:431
40. He JH, Sheng HW, Schilling PJ, Chien C-L, Ma E (2001) *Phys Rev Lett* 86:2826
41. Van Swygenhoven H, Caro A (1998) *Phys Rev B* 58:11246
42. Maxwell JC (1867) *Philos Trans R Soc Lon* 157:49
43. Nitta KH, Suzuki K (1999) *Macromol Theory Simul* 8:254
44. Casula G, Carcione JM (1992) *Boll Geofis Teor Appl* 34:235
45. Fan GJ, Choo H, Liaw PK, Lavernia EJ (2005) *Metall Mater Trans A* 36:2641
46. Frøseth A, Van Swygenhoven H, Derlet PM (2004) *Acta Mater* 52:2259
47. Li XY, Wei YJ, Lu L, Lu K, Gao HJ (2010) *Nature* 464:877
48. Daehn GS (2001) *Acta Mater* 49:2017
49. Radmilovic V, Miller MK, Mitlin D, Dahmen U (2006) *Scripta Mater* 54:1973
50. Kumar KS, Van Swygenhoven H, Suresh S (2003) *Acta Mater* 51:5743
51. Li H, Ebrahimi F, Choo H, Liaw PK (2006) *J Mater Sci* 41:7636. doi:[10.1007/s10853-006-0856-3](https://doi.org/10.1007/s10853-006-0856-3)
52. Voyiadjis GZ, Deliktas B (2010) *Acta Mech* 213:3
53. Horstemeyer MF, Baskes MI, Plimpton SJ (2004) *Acta Mater* 49:4363